2980 *Chem. Mater.* **2009,** *21,* 2980–2992
DOI:10.1021/cm900642p

CHEMISTRY OF MATERIALS
Article

Metallo-Supramolecular Nanospheres via Hierarchical Self-Assembly

H. Tarik Baytekin,[†] Bilge Baytekin,[†] Andrea Schulz,[†] Andreas Springer,[†] Thomas Gross,[‡] Wolfgang Unger,[‡] Marina Artamonova,[§] Sabine Schlecht,[§] Dieter Lentz,[§] and Christoph A. Schalley*,[†]

[†]*Institut für Chemie und Biochemie, Freie Universität, Berlin, Takustrasse 3, D-14195, Berlin, Germany,* [‡]*Bundesanstalt für Materialforschung und -prüfung, Unter den Eichen 44-46, 12203 Berlin, Germany, and* [§]*Institut für Chemie und Biochemie, Freie Universität, Berlin, Fabeckstrasse 34-36, D-14195, Berlin, Germany*

Received March 6, 2009. Revised Manuscript Received May 22, 2009

A novel coordination oligo/polymer is synthesized by metal-directed self-assembly from equimolar amounts of the (dppp)M(OTf)$_2$ precursor complexes (dppp = bis-(diphenylphosphino)-propane, OTf = triflate; M = Pd^{II} or M = Pt^{II}) and banana-shaped bidentate dipyridyl ligands. The assemblies were characterized by ESI mass spectrometry and NMR spectroscopy. The analysis of the cloudy suspension prepared by dissolving the coordination polymer in aqueous methanol solutions indicates nanosized spherical objects to form. Evidence for vesicle formation from these metallo-supramolecular oligomers comes from (cryogenic) transmission electron microscopy (TEM, cryo-TEM). Atomic force microscopy revealed stable nanospheres on hydrophilic mica and monolayer formation on hydrophobic highly oriented pyrolitic graphite (HOPG) substrates. On mica, also torus-shaped object were observed, which are rationalized by vesicles that opened during the drying procedure and released the internal solvent. Elemental analysis of the nanoassemblies by X-ray photoelectron spectroscopy (XPS) indicates uncoordinated and coordinated pyridines in the coordination polymers that form the nanospheres. Various control experiments using different metal centers and modified ligands support the conclusions.

Introduction

The spontaneous formation of higher-order structures from simpler building blocks by means of weak noncovalent interactions is fundamental to self-assembly.[1] Many complex architectures and phenomena in nature, such as the folding of proteins, the formation of bilayer membranes, or the winding up of nucleic acids into the DNA double helix are examples of self-assembly. Mimicry of nature's elaborate and complex functional architectures is likely impossible to be achieved by covalent synthesis. As stated by Feynman in the 1950s, the "bottom-up" approach[2] offers new promises to nanotechnology and chemists can benefit from self-assembly strategies. Metal-directed self-assembly makes use of directional coordinative bonds between the ligands and the metals to achieve well-designed multicomponent architectures in one, two, or three dimensions. Based on this coordination chemistry, successful strategies have been developed for the construction of highly elaborate structures. The advantage of metal-directed self-assembly is the control over different geometries and bond strengths depending on the metal ions or complexes utilized in the assembly.

A huge body of literature exists on a broad variety of nano-objects such as nanotubes,[3] vesicles,[4] or micelles,[5]

*Corresponding author. Fax: 49-(0)30-838-55817. Phone: 49-(0)30-838-52639. E-mail: schalley@chemie.fu-berlin.de.

(1) General reviews on self-assembly: (a) Whitesides, G. M.; Mathias, J. P.; Seto, C. T. *Science* **1991**, *254*, 1312–1319. (b) Philp, D.; Stoddart, J. F. *Angew. Chem.* **1996**, *108*, 1242–1286. *Angew. Chem., Int. Ed.* **1996**, *35*, 1154-1196. (c) Lehn, J.-M. *Science* **2002**, *295*, 2400–2403. (d) Vriezema, D. M.; Aragonès, M. C.; Elemans, J. A. A.W.; Cornelissen, J. J. L. M.; Rowan, A. E.; Nolte, R. J. M. *Chem. Rev.* **2005**, 1445–1489.

(2) Feynman, R. *Sat. Rev.* **1960**, *43*, 45–47.

(3) (a) Aoyagi, M.; Biradha, K.; Fujita, M. *J. Am. Chem. Soc.* **1999**, *121*, 7457–7458. (b) Kim, Y.; Mayer, M. F.; Zimmerman, S. C. *Angew. Chem.* **2003**, *115*, 1153–1158. *Angew. Chem., Int. Ed.* **2003**, *42*, 1121-1126. (c) Tashiro, S.; Tominaga, M.; Kusukawa, T.; Kawano, M.; Sakamoto, S.; Yamaguchi, K.; Fujita, M. *Angew. Chem.* **2003**, *115*, 5742–5745. *Angew. Chem., Int. Ed.* **2003**, *42*, 3267-3270. (d) Kim, D. H.; Karan, P.; Göring, P.; Leclaire, J.; Caminade, A.-M.; Majoral, J.-P.; Gösele, U.; Steinhart, M.; Knoll, W. *Small* **2005**, *1*, 99–102. (e) Shimizu, T.; Masuda, M.; Minamikawa, H. *Chem. Rev.* **2005**, *105*, 1401–1444. (f) Yamaguchi, T.; Tashiro, S.; Tominaga, M.; Kawano, M.; Ozeki, T.; Fujita, M. *Chem. Asian J.* **2007**, *2*, 468–476.

(4) (a) Yoshikawa, I.; Sawayama, J.; Araki, K. *Angew. Chem.* **2008**, *120*, 1054–1057. *Angew. Chem., Int. Ed.* **2008**, *47*, 1038-1041. (b) Boerakker, M. J.; Hannink, J. M.; Bomans, P. H. H.; Frederik, P. M.; Nolte, R. J. M.; Meijer, E. M.; Sommerdijk, N. A. J. M. *Angew. Chem.* **2002**, *114*, 4413–4415. (c) *Angew. Chem., Int. Ed.* **2002**, *41*, 4239-4241.

(5) (a) Draeger, C.; Böttcher, C.; Messerschmidt, C.; Schulz, A.; Ruhlmann, L.; Siggel, U.; Hammarström, L.; Berglund-Baudin, H.; Fuhrhop, J.-H. *Langmuir* **2000**, *16*, 2068–2077. (b) Messerschmidt, C.; Draeger, C.; Schulz, A.; Rabe, J. P.; Fuhrhop, J.-H. *Langmuir* **2001**, *17*, 3526–3531. (c) Kellermann, M.; Bauer, W.; Hirsch, A.; Schade, B.; Ludwig, K.; Böttcher, C. *Angew. Chem.* **2004**, *116*, 3019–3022. *Angew. Chem., Int. Ed.* **2004**, *43*, 2959-2962; (d) Ryu, J. -H.; Kim, H.-J.; Huang, Z.; Lee, E.; Lee, M. *Angew. Chem.* **2006**, *118*, 5430–5433. *Angew. Chem., Int. Ed.* **2006**, *45*, 5304-5307. (e) Yan, Y.; Besseling, N. A. M.; Keizer, A.; Marcelis, A. T. M.; Drechsler, M.; Stuart, A. C. *Angew. Chem.* **2007**, *119*, 1839–1841. *Angew. Chem., Int. Ed.* **2007**, *46*, 1807-1809; (f) Radowski, M. R.; Shukla, A.; von Berlepsch, H.; Böttcher, C.; Pickaert, G.; Rehage, H.; Haag, R. *Angew. Chem.* **2007**, *119*, 1287–1292. *Angew. Chem., Int. Ed.* **2007**, *46*, 1265-1269. (g) Maran, U.; Conley, H.; Frank, M.; Arif, A. M.; Orendt, A. M.; Britt, D.; Hlady, V.; Davis, R.; Stang, P. J. *Langmuir* **2008**, *24*, 5400–5410.

 Published on Web 06/17/2009

which have been prepared from many different molecules like inter alia synthetic amphiphilic block copolymers,[6] amphiphilic perylene bisimides,[7] porphyrins,[8] terpyridines,[9] β-cyclodextrin complexes,[10] zwitterionic guanidiniocarbonyl pyrrole carboxylate,[11] or inorganic transition metal-oxide clusters.[12] Only very recently, however, were the very first examples of metallo-supramolecular compounds reported that assemble hierarchically into vesicles.[13] Here, we present evidence for the formation of vesicles from novel coordination oligomers synthesized by metal-directed self-assembly of quite simple building blocks. These spherical nano-objects are characterized by different analytical techniques such as atomic force microscopy, (cryo-) transmission electron microscopy, and X-ray photoelectron microscopy.

Results and Discussion

1. Synthesis. Standard amide-bond formation between Hunter's diamine[14] **1** and isonicotinoyl chloride **2** yields the banana-shaped bidentate dipyridyl-substituted ligand **6** (Scheme 1A),[15] which bears two diverging coordination sites. The metallo-supramolecular polymers **11a** and **11b** can easily be prepared with yields of 95 and 90% by mixing equimolar amounts (0.4 mM) of ligand **6** and the (dppp)M(OTf)$_2$ precursors (dppp = bis-(diphenylphosphino)-propane, OTf = triflate; M = Pd^{II} (**10a**) or M = Pt^{II} (**10b**))[16] in 25 mL of CH_2Cl_2 or acetonitrile, stirring for 2 h, and precipitation of the products **11a** and **11b** by slow addition of diethyl ether (Scheme 1B).[17] It should be noted that each of the d^8 transition metal complexes connecting the ligands (the "connector") is doubly positively charged. The charges are counterbalanced by two triflate counterions, which according to X-ray studies[18] are usually bound electrostatically to the square-planar metal centers in the two apical positions.

Nanospheres **Sph-1a** and **Sph-1b** were prepared from the preformed and isolated coordination oligomers **11a** and **11b**, respectively (approach 1, Scheme 1C). However, direct mixing (approach 2, Scheme 1C) of the building blocks (ligand **6** with either **10a** or **10b** in aqueous methanol solution) resulted in similar nanospheres **Sph-2a** and **Sph-2a**, indicating that the nanospheres also form in a hierarchical self-assembly process directly from the starting compounds.

A selection of control compounds has also been prepared (Scheme 1A). Divalent ligand **8** carries the pyridine nitrogen atoms at a different ring position. Ligands **5** and **7** are monodentate with the ethyl pyridinium group in **7** mimicking the charged metal complex otherwise coordinated to the corresponding ligand **6**. Compound **9** represents a ligand bearing two charges, one on each pyridine, which again resemble a metal−ligand complex; however, without the ability to form growing chains. From ligands **8**, **5**, and **7**, assemblies **12a,b**, **13a,b**, and **14a,b** were prepared without intermediate isolation of the metallo-supramolecular polymers by directly mixing the building blocks (approach 2) in 40% aqueous methanol solution. Finally, assemblies **16a,b** were prepared by mixing a stock solution of water-soluble metal connectors (**15a** and **15b)** and ligand **6** in water.

2. Crystal Structure of Ligand 6. X-ray-quality single crystals of ligand **6** have been obtained from a saturated solution of **6** in acetonitrile at 25 °C after standing for one day in a closed vial. To avoid the loss of solvent molecules, we performed the data collection at −130 °C.

(6) (a) Discher, D. E.; Eisenberg, A. *Science* **2002**, *297*, 967–973. (b) Opsteen, J. A.; Cornelissen, J. J. L. M.; Hest, J. C. M. V. *Pure. Appl. Chem.* **2004**, *76*, 1309–1319. (c) Shklyarevskiy, I. O.; Jonkheijm, P.; Christianen, P. C. M.; Schenning, A. P. H. J.; Meijer, E. W.; Henze, O.; Kilbinger, A. F. M.; Feast, W. J.; Guerzo, A. D.; Desvergne, J.-P.; Maan, J. C. *J. Am. Chem. Soc.* **2005**, *127*, 1112–1113. (d) Tian, L.; Nguyen, P.; Hammond, P. T. *Chem. Commun.* **2006**, 3489–3491.

(7) Zhang, X.; Chen, Z.; Würthner, F. *J. Am. Chem. Soc.* **2007**, *129*, 4886–4887.

(8) (a) Ghoroghchian, P. P.; Frail, P. R.; Susumu, K.; Blessington, D.; Brannan, A. K.; Bates, F. S.; Chance, B.; Hammer, D. A.; Therien, M. J. *Proc. Natl. Acad. Sci. U.S.A.* **2005**, *102*, 2922–2927. (b) Li, Y.; Li, X.; Li, Y.; Liu, H.; Wang, S.; Gan, H.; Li, J.; Wang, N.; He, X.; Zhu, D. *Angew. Chem.* **2006**, *118*, 3721–3725. *Angew. Chem., Int. Ed.* **2006**, *45*, 3639-3643.

(9) (a) Messerschmidt, C.; Draeger, C.; Schulz, A.; Rabe, J. P.; Fuhrhop, J.-H. *Langmuir* **2001**, *17*, 3526–3531. (b) Gohy, J.-F.; Lohmeijer, B. G. G.; Schubert, U. S. *Macromolecules* **2002**, *35*, 4560–4563. (c) Gohy, J.-F.; Lohmeijer, B. G. G.; Décamps, B.; Leroy, E.; Boileau, S.; van den Broek, J. A.; Schubert, D.; Haase, W.; Schubert, U. S. *Polym. Int.* **2003**, *52*, 1611–1618.

(10) (a) Vriezema, D. V.; Hoogboom, J.; Velonia, K.; Takazawa, K.; Christianen, P. C. M.; Maan, J. C.; Rowan, A. E.; Nolte, R. J. M. *Angew. Chem.* **2003**, *115*, 796–800. *Angew. Chem., Int. Ed.* **2003**, *42*, 772-776. (b) Liu, Y.; Xu, J.; Craig, S. L. *Chem. Commun.* **2004**, 1864–1865. (c) Zou, J.; Tao, F.; Jiang, M. *Langmuir* **2007**, *23*, 12791–12794. (d) Jin, B.; Chen, X.; Wang, X.; Yang, C.; Xie, Y.; Qiu, H. *Chem.—Eur. J.* **2007**, *13*, 9137–9142. (e) Wang, Y.; Ma, N.; Wang, Z.; Zhang, X. *Angew. Chem.* **2007**, *119*, 2881–2884. *Angew. Chem., Int. Ed.* **2007**, *46*, 2823-2826. (f) Chiper, M.; Meier, M. A. R.; Wouters, D.; Hoeppener, S.; Fustin, C.-A.; Gohy, J.-F.; Schubert, U. S. *Macromolecules* **2008**, *41*, 2771–2777.

(11) Rehm, T.; Stepanenko, V.; Zhang, X.; Würthner, F.; Gröhn, F.; Klein, K.; Schmuck, C. *Org. Lett.* **2008**, *10*, 1469–1472.

(12) (a) Liu, T.; Diemann, E.; Li, H.; Dress, A. W. M.; Müller, A. *Nature* **2003**, *426*, 59–62. (b) Liu, T. *J. Am. Chem. Soc.* **2003**, *125*, 312–313. (c) Roy, S.; L. C; Bossers, A.; Meeldijk, H. J.; Kuipers, B. W.; Kegel, W. K. *Langmuir* **2008**, *24*, 666–669. (d) Liu, T.; Imber, B.; Diemann, E.; Liu, G.; Cokleski, K.; Li, H.; Chen, Z.; Müller, A. *J. Am. Chem. Soc.* **2006**, *128*, 15914–15920.

(13) (a) Li, D.; Zhang, J.; Landskron, K.; Liu, T. *J. Am. Chem. Soc.* **2008**, *130*, 4226–4227. (b) Moughton, A. O.; O'Reilly, R. K. *J. Am. Chem. Soc.* **2008**, *130*, 8714–8725. (c) Rieter, W. J.; Pott, K. M.; Taylor, K. M. L.; Lin, W. *J. Am. Chem. Soc.* **2008**, *130*, 11584–11585.

(14) (a) Hunter, C. A. *J. Am. Chem. Soc.* **1992**, *114*, 5303–5311. (b) Hunter, C. A.; Jones, P. S.; Tiger, P.; Tomas, S. *Chem.—Eur. J.* **2002**, *8*, 5435–5446.

(15) Hunter, C. A.; Low, C. M. R.; Rotger, C.; Vinter, J. G.; Zonta, C. *Proc. Natl. Acad. Sci. U.S.A.* **2002**, *99*, 4873–4876.

(16) (a) Stang, P. J.; Cao, D. H. *J. Am. Chem. Soc.* **1994**, *116*, 4981–4982. (b) Stang, P. J.; Whiteford, J. A. *Organometallics* **1994**, *13*, 3776–3777. (c) Stang, P. J.; Cao, D. H.; Saito, S.; Arif, A. M. *J. Am. Chem. Soc.* **1995**, *117*, 6273–6283. (d) Olenyuk, B.; Whiteford, J. A.; Stang, P. *J. Am. Chem. Soc.* **1996**, *118*, 8221–8230. (e) Chatterjee, B.; Noveron, J. C.; Resendiz, M. J. E.; Liu, J.; Yamamoto, T.; Parker, D.; Cinke, M.; Nguyen, C. V.; Arif, A. M.; Stang, P. *J. Am. Chem. Soc.* **2004**, *126*, 10645–10656.

(17) (a) Constable, E. C.; Meier, W.; Nardin, C.; Mundwiler, S. *Chem. Commun.* **1999**, 1483–1484. (b) Qin, Z.; Jennings, M. C.; Puddephatt, R. *Chem. Commun.* **2002**, 354–355. (c) Burchell, T. J.; Eisler, D. J.; Puddephatt, R. J. *Chem. Commun.* **2004**, 944–945. (d) Kim, H.-J.; Zin, W.-C.; Lee, M. *J. Am. Chem. Soc.* **2004**, *126*, 7009–7014. (e) Wackerly, J. Wm.; Moore, J. S. *Macromolecules* **2006**, *39*, 7269–7276. (f) Maeda, H.; Hasegawa, M.; Hashimoto, T.; Kakimoto, T.; Nishio, S.; Nakanishi, T. *J. Am. Chem. Soc.* **2006**, *128*, 10024–10025.

(18) Weilandt, T.; Troff, R. W.; Saxell, H.; Rissanen, K.; Schalley, C. A. *Inorg. Chem.* **2008**, *47*, 7588–7598.

Scheme 1. (A) Organic Synthesis of the Ligands Involved in This Study; (B) Formation of Assemblies from Organo-Soluble (dppp) $M^{II}(O_3SCF_3)_2$ complexes 10a,b (red) and Ligands 5−8 (top); Formation of Water-Soluble Assemblies from (en)$M^{II}(NO_3)_2$ Complexes 15a,b (blue) and 6 (bottom); (C) Preparation of the Vesicles with (approach 1) and without (approach 2) Intermediate Isolation of the Oligomeric Assembly ("Sph-1a", for example, stands for spherical nano-objects formed from 11a according to approach 1 containing (dppp)Pd^{II} as the metal ion)[a]

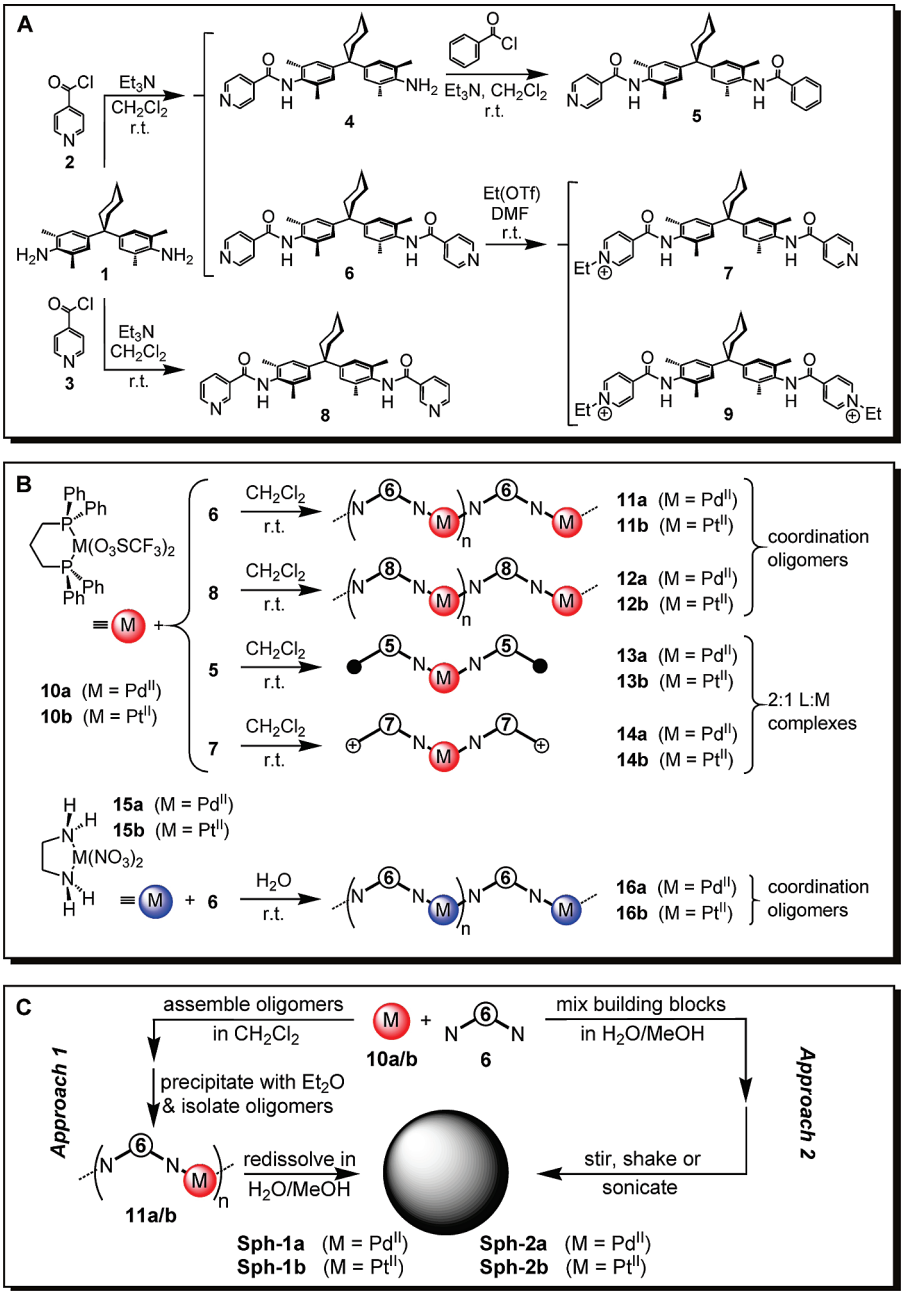

[a] Pd^{II} is always denoted by adding "**a**" to the compound number, Pt^{II} by adding "**b**". For clarity, the cartoons corresponding to the ligands carry the ligands' numbers.

The molecular structures of two independent ligand molecules (A and B) present in the unit cell are shown in Figure 1. The distances between two pyridine nitrogen atoms in the same molecule are 15.16 Å (molecule A) and 17.36 Å (molecule B), those between the pyridine nitrogens and the central carbon atom are 10.82 and 10.79 Å in molecule A and 10.79 and 10.80 Å in molecule B. The CCC bond angles θ are 108.05 (molecule A) and 104.69° (molecule B). Because of conjugation, the pyridine rings are almost coplanar with the carbonyl groups of the amide groups. These data show both molecules to differ to some extent most likely due to packing effects that deform both to small but different extents. The distance between the centroids of the two almost coplanar pyridine rings of two neighboring molecules is 8.30 Å (see the Supporting Information for crystallographic details).

3. Mass Spectrometric Characterization of Coordination Oligomers. Molecular modeling predicts the ligand's curvature to be not ideal for the formation of small 2:2 macrocycles from (dppp)$M(OTf)_2$ connectors and ligands. One might expect a mixture of coordination oligomers to form, avoiding the resulting strain. This is

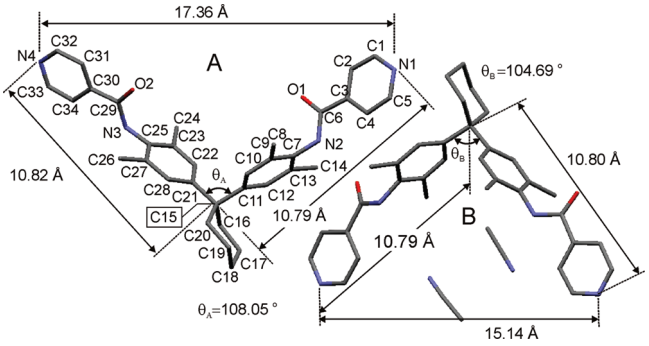

Figure 1. Molecular structure of (A) ligand **6** with (B) a neighboring ligand. Hydrogen atoms are removed for clarity.

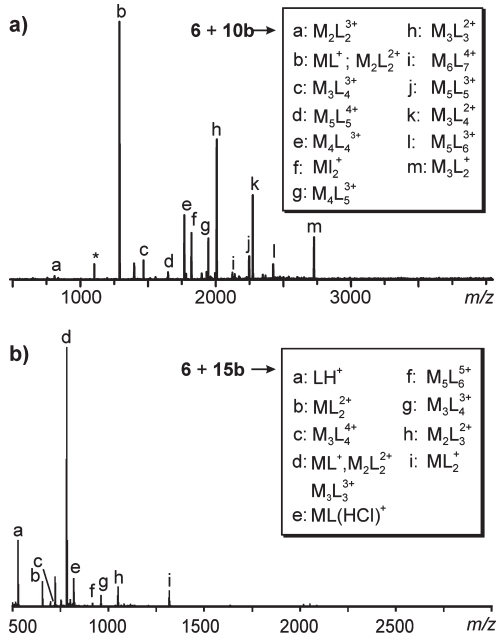

Figure 2. ESI-FTICR mass spectra of (a) a 150 μM acetone solution of **11b** and (b) a 150 μM acetone: water (10: 1) solution of **16b**. The asterisk indicates an instrument artifact from stray radiation.

confirmed by electrospray ionization mass spectrometry (ESI-MS).[19] For oligomer **11b**, a quite complex mass spectrum is obtained (Figure 2a), from which three main conclusions can be drawn. (i) Oligomers are observed up to the $M_6L_7^{4+}$ complex; assembly formation is thus not restricted to small cycles. (ii) All signals except the signal denoted "m" in Figure 2 (likely a fragment) either correspond to probably cyclic oligomers with the same number of metal centers and ligands (M:L = 2:2, 3:3, 4:4, 5:5) or to linear oligomers, each bearing one ligand more than metal connectors (M:L = 1:2, 2:3; 3:4, 4:5, 5:6, 6:7). This is in line with the somewhat higher binding energy of the second pyridine at each metal center.[20] (iii) Fragmentation may occur during ionization[21] so that the oligomer chains may be longer in solution. Also, larger complexes appear usually as less intense signals than smaller ones for technical reasons. Similar results are obtained for the analogous Pd^{II} compound **11a**.

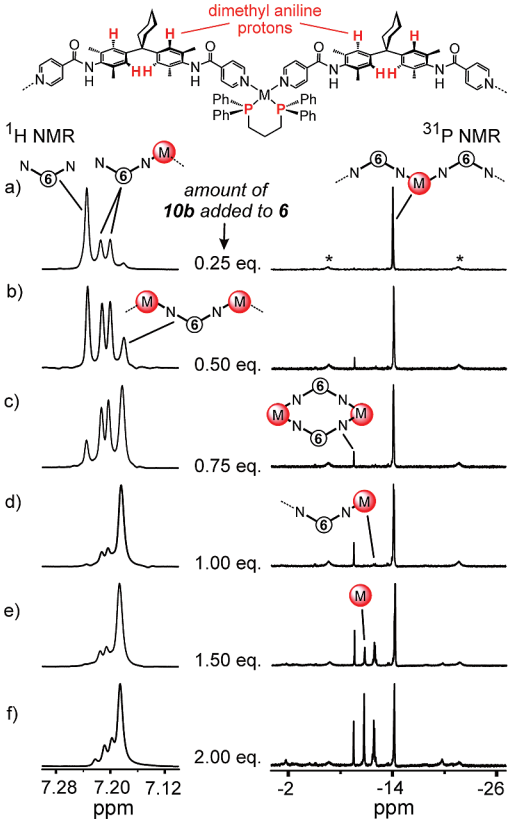

Figure 3. Left: Partial ^{1}H NMR spectra of mixtures of ligand **6** with increasing amounts of **10b** ([D_7]DMF at 298 K). Only the signals for the aromatic dimethylaniline protons are shown (red in the structure on top) which indicate the coexistence of free, singly, and doubly coordinated ligands **6**. Right: ^{31}P NMR spectra of the same samples ([D_7]DMF at 298 K). The singly substituted metal center bears two different P atoms and can be easily identified by the two close doublet signals. Asterisks mark the ^{195}Pt satellites ($^1J_{P-Pt}$ coupling), which are quite sensitive to pyridine coordination.

If the organo-soluble (dppp)Pt^{II} connector is replaced by its water-soluble equivalent (en)M^{II}, the mass spectrum again showed the formation of coordination oligomers. This time, the oligomeric species appear to have lengths shorter than those of the assemblies with (dppp) M^{II} metal connectors. The reason might be either the formation of shorter assemblies in solution because of the lack of the stabilizing $\pi-\pi$ interactions between the dppp phenyl rings at the metal connector and the coordinating pyridine rings, or more pronounced fragmentation during ionization.

4. ^{1}H and ^{31}P NMR Characterization of 11a,b. An NMR titration of Pt^{II} complex **10b** into a solution of ligand **6** provides complementary results indicating oligomer formation. The formation of the assemblies can be monitored by ^{1}H and ^{31}P NMR spectroscopy (Figure 3). At low metal complex concentrations (Figure 3a), one ^{1}H NMR signal is observed for the aromatic dimethylaniline protons of free ligand **6** next to two signals (1:1 ratio) for singly coordinated and thus unsymmetrical ligands. All metal centers are doubly coordinated, rendering the

(19) Baytekin, H. T.; Sahre, M.; Rang, A.; Engeser, M.; Schulz, A.; Schalley, C. A. *Small* **2008**, *4*, 1823–1834.
(20) Würthner, F.; You, C.-C.; Saha-Möller, C. R. *Chem. Soc. Rev.* **2004**, *33*, 133–146.
(21) (a) Schalley, C. A.; Müller, T.; Linnartz, P.; Witt, M.; Schäfer, M.; Lützen, A. *Chem.—Eur. J.* **2002**, *8*, 3538–3551. (b) Engeser, M.; Rang, A.; Ferrer, M.; Gutierrez, A.; Baytekin, H. T.; Schalley, C. A. *Int. J. Mass Spec.* **2006**, *255*, 185–194.

P atoms equivalent; only one signal is observed in the ^{31}P NMR spectrum. Pyridine coordination is confirmed by a $^{1}J_{P-Pt}$ coupling constant of 3041 Hz ((dppp)Pt$(OTf)_2$ precursor: 3647 Hz). The NMR titration was performed in [D_7]-DMF at 298 K, because sharper signals were obtained in this solvent as compared to CD_2Cl_2. Upon increasing metal complex concentration, an additional aromatic phenylene ^{1}H NMR singlet for doubly coordinated ligands appears at 7.18 ppm, which grows to become the major one at a metal: ligand ratio of 1:1. At this point, all metal centers are still doubly substituted in line with the mass spectra discussed above. The additional small peak in the ^{31}P NMR spectrum appearing downfield from the major one may be due to strained cyclic 2:2 assemblies. At higher metal complex concentrations, singly substituted complexes appear as double doublets because of the two nonequivalent, mutually coupling P atoms. A singlet for free **10b** becomes also visible. At a 1:1 stoichiometry of metal and ligand at 298 K in [D_7]-DMF, the Pt^{II} assembly results in two sets of pyridine *ortho*-protons at 9.27 and at 8.83 ppm assigned to the *ortho*-protons of the pyridines that are coordinated and uncoordinated to the metal center, respectively. The integral ratio of these two signals is around 8.8 when 1 equivalent of metal complex is used (Figure S1a in the Supporting Information). The intensity of free pyridine *ortho*-protons at 8.83 ppm decreases upon increasing metal complex concentration to 1.5 equivalents. Analogously, the pyridine *meta*-protons appear as two doublets at 7.97 and 7.86 ppm (superimposed with *dppp*-phenyl signals) for the 1:1 metal:ligand ratio. Mass spectrometry and NMR spectroscopy thus agree with each other indicating coordination oligomers to be formed. In line with earlier data, ligand exchange is fast on the NMR time scale at r.t. for the corresponding Pd^{II} compound **11a**. Only one averaged set of signals is observed (Figure S1b in the Supporting Information). Similarly, the ^{1}H NMR spectra of **16b** indicate oligomeric assemblies to form in [D_6]-DMSO at 298 K.

Temperature-dependent changes in ^{1}H NMR spectra have been reported for many metal-directed supramolecular self-assembled systems. For **11a**, temperature-dependent ^{1}H NMR spectra indicate a dynamic ligand exchange process (Figure 4). The Pd^{II} assembly results in one set of signals at 300 K in [D_7]-DMF (Figure 4a). The pyridine ortho-protons give rise to a quite broad signal already indicating that a dynamic process may occur. An additional signal appearing as a shoulder to this peak appears at ca. 8.9 ppm at 265 K (Figure 4b). At even lower temperatures (223 K), a larger, broad signal (i), a shoulder (ii) attached to it on the right, and a less intense, sharp proton signal (iii) appear in the same region of the spectrum (Figure 4c). They can be assigned to (i) the pyridines of the ligands that are coordinated to the metal center on both sides and (ii) and (iii) to the pyridine rings of a singly coordinated ligand at the end of a linear coordination oligomer chain. Similar to the signals of the ortho-protons, the amide protons give rise to a shoulder, indicating different amide groups to exist in solution.

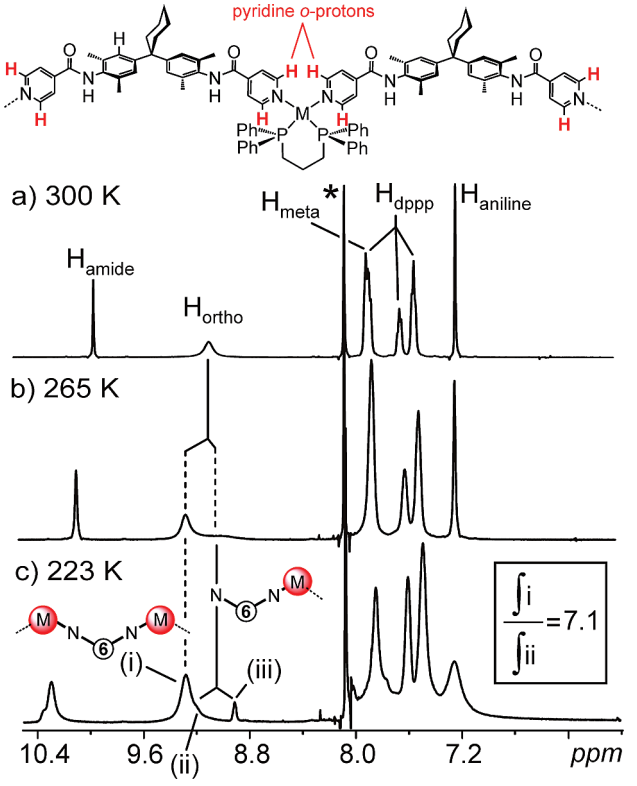

Figure 4. ^{1}H NMR spectra of **11a** in [D_7]-DMF at (a) 300, (b) 265, and (c) 223 K. The asterisk indicates the [D_7]-DMF signal. At lower temperatures, the pyridine ortho-protons exhibit coalescence and several sets of signals are observed below the coalescence temperature in close analogy to **11b**.

The ratio of the two cannot be determined precisely, but it seems to be in the same order of magnitude as that for the (i) and (iii). From these results, we conclude that an analogous situation exists for the Pd^{II} and Pt^{II} assemblies **11a** and **11b**. The exchange rates, however, are quite different for the two metals.[18]

5. TEM Characterization of Self-Assembled Nanospheres. When preassembled metallo-supramolecular polymers **11a** or **11b** are dissolved in methanol and heated to 50 °C followed by cooling to r.t. and dropwise addition of deionized water, a cloudy suspension is obtained (Scheme 1C, approach 1). The same happens when the building blocks are treated the same way without intermediate isolation of the coordination oligomers (approach 2). Because we suspected vesicles or micelles to form, TEM images were recorded. After blotting the Pd^{II} assemblies on collodium-coated copper grids vapor-coated with a carbon-film, the TEM images revealed spherical objects to form (Figure 5c). The corresponding Pt^{II} complexes form similar objects, which are somewhat smaller in diameter and more homogeneous in size (Figure 5d). Sonication of the samples did not change the result much regardless of the metal cation used. Cryo-TEM images (Figures 5a,b) reveal two different kinds of spherical object to be present for both the Pd^{II} and Pt^{II} assemblies **Sph-2a** and **Sph-2b**: Small ones with diameters of 40−50 nm that do not show contrast differences between the interior and the outer shell are completely filled. Much larger nanospheres with diameters greater

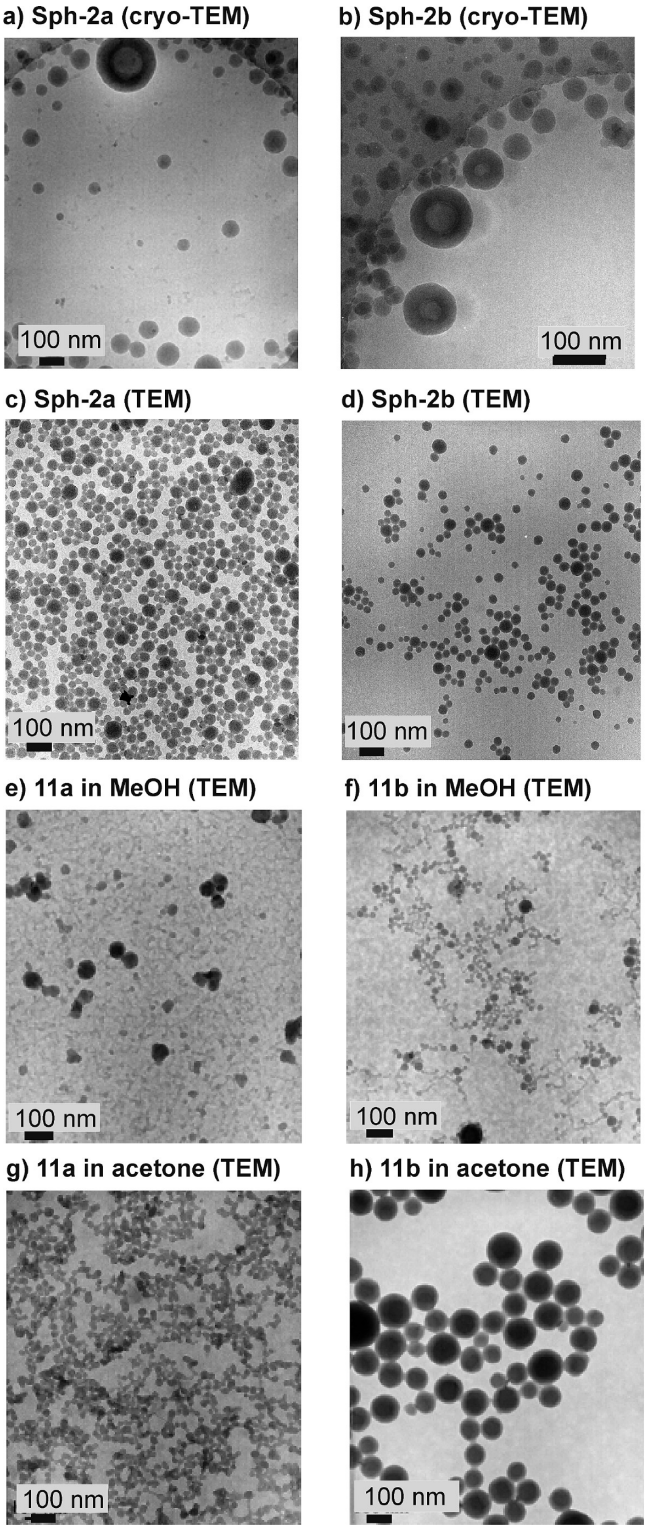

Figure 5. (a, b) Representative cryo-TEM images of **Sph-2a** and **Sph-2b** in 60:40 water/methanol. No drying step is involved in the sample preparation. (c, d) Same samples, but noncryo-TEM image. Sample preparation involves a drying step. (e, h) The same assemblies **11a,b** are used, but the samples were prepared in different solvents: (e, f) pure methanol, (g, h) acetone.

than ca. 100 nm have distinctly lower contrast at the center, implying the formation of vesicles with wall thicknesses of ca. 40 nm. It should be noted that the cryo-TEM is performed on frozen solutions that were propelled into liquid ethane and that the objects observed in these images have not undergone a drying process such as those seen in the conventional TEM images. Consequently, the objects observed in Figure 5a and b represent as closely as possible those occurring in solution.

Metallo-supramolecular polymers **11a,b** that were prepared in pure methanol and acetone were also investigated by TEM (Figure 5e−h). TEM images of nanospheres deposited from methanol (1 mg/mL) and acetone (2 mg/mL) also show both types of spherical objects, which sometimes tend to fuse into networks of nanospheres (Figure 5e−g).

6. TEM Control Experiments. The following control experiments have been performed: (i) Pt^{II} complex **10b** gave much smaller black dots in the TEM images, probably nanocrystals (Figure 6a). (ii) Bidentate ligand **6** alone leads to monolayer formation, when treated the same way (Figure 6b). (iii) Monodentate ligand **7**, which may mimic the positively charged metal center by an ethyl-pyridinium moiety, results in randomly distributed aggregates (Figure 6c). (iv) Bis-pyridinium salt **9** alone results in irregular aggregates that only became visible in the TEM after staining with phosphotungstic acid solution (Figure 6d). (v) Assemblies **13a,b** that are formed by mixing metal complexes **10a,b** and monodentate ligand **5** result in monolayered structures (Figure 6e, f). (vi) Similarly, assemblies **14a,b** that are prepared by mixing metal complexes **10a,b** and monodentate ligand **7** result in distorted, spherical, and irregular aggregates as well as monolayered structures (Figure 6g, h). (vii) Assemblies that are formed by mixing metal complexes **10a,b** and bidentate ligand **8** result in crystalline monolayered structures of coordination oligomers **12a,b** (Figure 6i, j). Very rarely, some spherical objects can be observed which are similar to the nanospheres described in this article (inset in Figure 6j and Figure S3 in the Supporting Information). (viii) The use of ligand **6** together with water-soluble $(en)M(NO_3)_2$ metal connectors[22] (**15a**: M = Pd^{II}; **15b**: M = Pt^{II}) yields coordination oligomers **16a,b**, which did not lead to the formation of any spherical objects.

From these control experiments, we conclude the presence of both bidentate ligand **6** and organo-soluble $(dppp)M(OSO_2CF_3)$ (**10a**: M = Pd^{II}; **10b**: M = Pt^{II}) connectors to be a prerequisite for nanosphere formation in aqueous methanol solution. Also, the structural details are important, e.g., the position of the pyridine nitrogen atom and the nature of the cis-blocking ligand (dppp vs en) on the metal centers. Finally, the formation of oligomer chains must be of importance for vesicle formation, because no nanospheres are observed with monodentate ligands **5** and **7** coordinated to $(dppp)M^{II}$ metal complexes.

7. AFM Characterization of Self-Assembled Nanospheres Deposited on HOPG and Mica. We investigated air-dried self-assembled nanospheres on hydrophobic

(22) (a) Fujita, M.; Yazaki, J.; Yamaguchi, K.; Ogura, K. *J. Am. Chem. Soc.* **1990**, *112*, 5645–5647. (b) Fujita, M.; Ibukura, F.; Yamaguchi, K.; Ogura, K. *J. Am. Chem. Soc.* **1995**, *117*, 4175–4176.

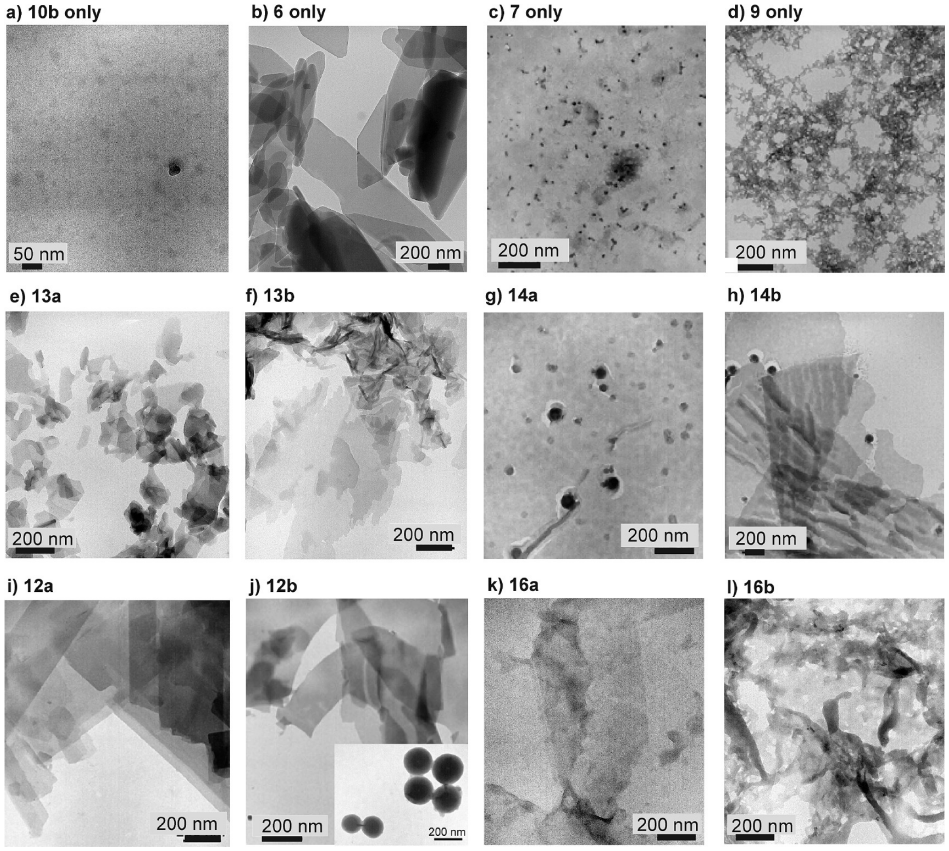

Figure 6. Representative TEM images of the control compounds indicated above each image. The samples were treated the same way as the nanospheres in Figure 5. The solvent is 60:40 water/methanol for samples a−j and 50:50 water/methanol for k and l.

HOPG and hydrophilic mica substrate by tapping-mode AFM. Metal complex **10b** and bidentate ligand **6** were first dissolved in acetone (where they also form nanospheres and vesicles as shown in Figure 5) and then deposited on one of the two substrates by blotting a drop of the acetone solution after 4 s at ambient atmosphere. At high concentrations, a fully covered surface of assemblies is obtained on HOPG substrate (Figure 7a). Dilution of the solution to one tenth with pure acetone (0.01 mg/mL), results in partial coverage of the surface forming a network on HOPG (Figure 7b). The height profile (Figure 7c) indicates a ca. 2.5 nm high incomplete monolayer over a large area. Some higher aggregates whose height is nearly twice that of the monolayer (inset (i) in Figure 7b) are observed and indicate a second layer on top of the first one. A surface fully covered with spherical objects is observed at higher concentration on more polar mica substrate (Figure 7d). Unlike the assemblies that are deposited on HOPG at high concentration, spherical and probably fused assemblies are deposited on mica. At low concentration (0.01 mg/mL), however, both spherical and torus-shaped[23] nano-objects were observed on mica (Figure 7e). Among the spherical objects, smaller spheres exist that are never torus-shaped. In addition, larger spheres occur that are in the size range comparable to that obtained from the TEM images for the vesicles. Their diameter appears to be increased to some extent, whereas the height is smaller than the diameter observed in the TEM images. This flattening can easily be rationalized by favorable interactions between the polar mica surface with the polar periphery of the vesicles. Some of these larger objects are torus-shaped. These nano-objects were found to be stable on the substrate surface even after 24 h.

We interpret these results as follows: The AFM experiments indicate different adsorption behavior of the assemblies to occur on both substrate surfaces because of the different surface polarities.[24] The vesicles and nanospheres observed in the TEM images have a polar surface that mediates the acetone contacts when dispersed in this solvent or the water/methanol contacts when prepared in mixtures of these solvents. Similarly, they survive when deposited on the polar mica. However, when the substrate is the nonpolar HOPG, the nonpolar parts from the inside of the vesicle walls are turned toward the surface. Finally, the vesicles and nanospheres are destroyed and films prevail. If we assume the nonpolar dppp phenyl groups to mediate the interaction with the HOPG with the ligands standing more or less upright in a reasonably well-ordered arrangement within the film, modeling predicts a height of ca. 2.6 nm for the film. This is in good agreement with the height of the monolayer as obtained from the AFM experiments.

The fact that only the larger spheres observed on the AFM substrate also appear as torus-shaped objects, while

(23) Antonietti, M.; Förster, S. *Adv. Mater.* **2003**, *15*, 1323–1333.

(24) Rakhmatullina, E.; Meier, W. *Langmuir* **2008**, *24*, 6254–6261.

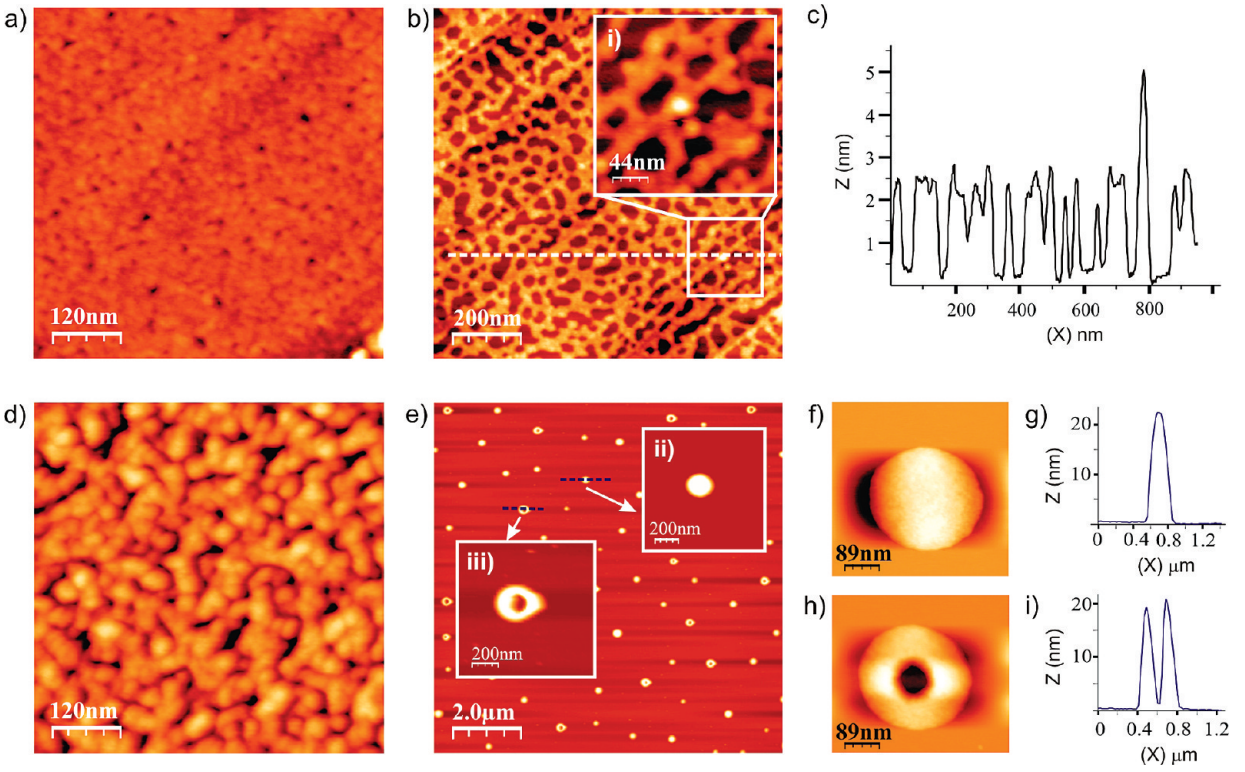

Figure 7. TM-AFM height image of the acetone solutions of the Pt^{II} assemblies **Sph-2b** deposited on (a, b) freshly cleaved HOPG and (d−h) mica. The concentrations of the assemblies are: 0.1 mg/mL in a and d; 0.01 mg/mL in b and e. (c) Height profile of the film on HOPG along the dotted line in b and its inset; (g, i) height profiles of the assemblies shown in insets (ii) and (iii) along the dotted lines indicated in e. (f, h) Magnified height images of nanosphere and the torus-shaped nano-objects.

the smaller ones never do, is in agreement with the cryo-TEM images: The smaller spheres did not show any contrast differences between the inside and wall and are therefore completely filled. When deposited on mica, they remain flattened, oblate-shaped, but well-rounded objects. In contrast, the larger spheres showed a contrast difference in the cryo-TEM images indicating them to contain a solvent-filled cavity inside. When they are deposited on mica and afterward dried, some of them survive the drying procedure because of the quite large wall thickness (ca. 40 nm, see above), whereas some of them open, release the interior solvent, and then appear as torus-shaped nano-objects. Both pieces of evidence, the cryo-TEM and the AFM experiments, thus strongly support the large spheres to be vesicles.

8. Powder X-ray Analyses of 11a,b and Self-Assembled Nanospheres Sph-2a,b. Powder X-ray experiments were performed with (i) the metallo-supramolecular polymers **11a** and **11b** as obtained by mixing the building blocks in dichloromethane and evaporating the solvent after assembly formation, (ii) by collecting the nanospheres **Sph-2a** and **Sph-2b** by centrifugation of a 2:3 methanol:water mixture, and (c) by depositing them from an acetone solution. In all cases, amorphous material was obtained as reflected in the structure-less powder X-ray diffractograms (see Figure S6 in the Supporting Information).

9. XPS Characterization of Self-Assembled Nanospheres Sph-1a,b. The elemental compositions of Pd^{II} and Pt^{II} metallo-nanospheres **Sph-1a** and **Sph-1b** were determined from X-ray photoelectron (XPS) spectra

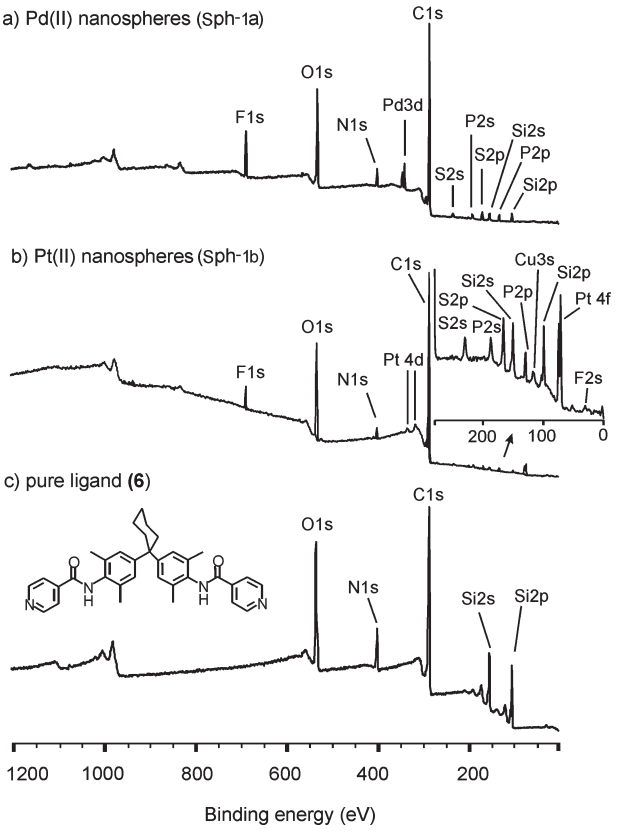

Figure 8. XPS survey spectra of (a) **Sph-1a** and (b) **Sph-1b** on TEM grids, and (c) pure ligand **6** deposited on a silicon wafer. The high amount of silicon in the XPS spectrum of **6** is due to this substrate.

Table 1. XPS-Derived Elemental Composition of Metal Complexes, (dppp)M(TfO)$_2$ (M = Pd^{II} 10a and Pt^{II} 10b), and Nanospheres As Prepared in Aqueous Methanol Solutions

	at %								
samples	Pd	Pt	N	P	O	C	F	S	N:metal ratio
10a	1.7			2.6	17.5	59.7	12.7	3.8	
10b		1.2		1.9	18.5	42.5	15.3	1.5	
Sph-1a (60:40 H_2O/MeOH)	0.8		3.8	1.4	13.4	71.3	4.9	1.6	4.8
Sph-2a (40:60 H_2O/MeOH)	0.5		2.8	0.8	15.1	73.7	3.0	0.8	5.6
Sph-1b (60:40 H_2O/MeOH)		0.8	3.0	1.9	11.7	66.2	7.3	2.9	3.8

(Figure 8a,b). Atomic percentages (at %) of the elements are given in Table 1 for the organo-soluble dpppPd^{II} and dpppPt^{II} metal complexes **10a,b** and the nanospheres **Sph-1a,b**. The same collodium-coated copper grids that were used as substrates in the TEM experiments for **Sph-1a,b** were used in the XPS measurements. Therefore, high amounts of carbon are detected because of the carbon film on the copper grid; the high content of oxygen is due to solvent molecules (water and methanol) that are presumably trapped inside the nanospheres. Although the uncertainty is quite high, quantification of Pd(3d), Pt(4f), and N(1s) peaks in XPS survey spectra indicate the formation of oligomeric assemblies since in either case N/Pd or N/Pt atomic ratios are found to be higher than four. This indicates the presence of ligand-terminated chains. As a test case, the elemental compositions of organo-soluble metal complexes (dppp)Pd(TfO)$_2$ **10a** and (dppp)Pt(TfO)$_2$ **10b** were also confirmed by quantification of XPS survey spectra within the error limits of XPS (see Figure S7 in the Supporting Information).

XPS can also provide information about metal−ligand bond formation by monitoring the chemical shifts in the characteristic binding energy of the corresponding metal and heteroatoms. Moreover, the appearance of new or disappearance of existing (sub)peaks upon formation of assemblies allows us to follow structural changes. So far, a rather limited number of studies have been published[25] in which core level XPS information is used to follow the formation of metallo-supramolecular assemblies.

Coordination of ligand **6** to **10a** and **10b** can clearly be monitored by changes in high-resolution XPS N1s spectra.[26] The N1s region of the XPS spectrum of free ligand **6** prepared on a silicon wafer is constituted by several N1s subpeaks originating from (i) free pyridine nitrogen, (ii) amide nitrogen,[27] (iii) weakly and (iv) strongly H-bonded pyridine nitrogen,[27a] and (v) protonated pyridine nitrogen atoms[28a] (Figure 9a). Comparison of the N1s spectrum of the free ligand with that of the assemblies reveals that the intensities of N1s peaks that originate from both H-bonded or protonated nitrogens is significantly reduced for the nanospheres **Sph-1a** and **Sph-1b** (Figure 9b−d). Upon the formation of metallo-supramolecular assemblies, the N1s peak of the free nitrogen on the pyridine ring disappears and consequently the numbers of the protonated nitrogens and the nitrogen atoms that form H-bonding decrease, too (Figure 9b−d). For the nanospheres **Sph-1a,b**, the N1s peaks can be fitted by three subpeaks; two subpeaks originate from the ligand itself (pyridine and amide nitrogens). The new peak that appears at ca. 399.6 eV is indicative of a nitrogen on the pyridine ring that is coordinated to the metal centers (Figure 9b−d). Binding energy data of high-resolution N1s component peaks measured with the nanospheres **Sph-1a,b** and pure ligand **6** are given in Table 2.

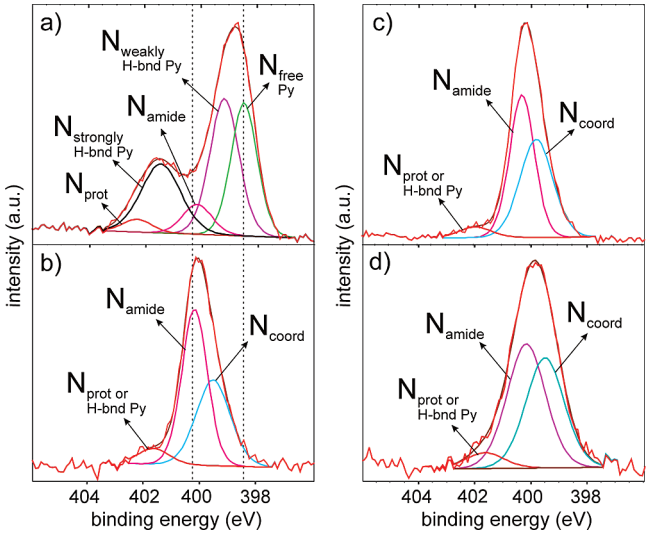

Figure 9. Detailed analysis of highly resolved N1s XPS spectra of the ligand and Pd^{II} or Pt^{II} nanospheres. (a) Ligand **6**, (b) **Sph-1a** from 60:40 H_2O/MeOH solution, (c) **Sph-2a** from 40:60 H_2O/MeOH solution, and (d) **Sph-1b** from 60:40 H_2O/MeOH solution.

10. pH Dependence. The vesicles form under conditions close to neutral pH. When trifluoromethane sulfonic acid was added, the vesicles disintegrate and a precipitate forms. Most likely, the pyridines are protonated and the

(25) (a) Sarno, D. M.; Jiang, B.; Grosfeld, D.; Afriyie, J. O.; Matienzo, L. J.; Jones, W. E.Jr. *Langmuir* **2000**, *16*, 6191–6199. (b) Zubavichus, Y.; Zharnikov, M.; Yang, Y.; Fuchs, O.; Umbach, E.; Heske, C.; Ulman, A.; Grunze, M. *Langmuir* **2004**, *20*, 11022–11029. (c) Li, H.; Xu, B.; Evans, D.; Reutt-Robey, J. E. *J. Phys. Chem.* **2007**, *111*, 2102–2106. (d) Busi, M.; Laurenti, M.; Condorelli, G. G.; Motta, A.; Favazza, M.; Fragalà, I. L.; Montalti, M.; Prodi, L.; Dalcanale, E. *Chem.—Eur. J.* **2007**, *13*, 6891–6898.

(26) (a) Tokuhisa, H.; Kanesato, M. *Langmuir* **2005**, *21*, 9728–9732. (b) Bradley, T. J.; Schfield, W.C. E.; Garrod, R. P.; Badyal, J. P. S. *Langmuir* **2006**, *22*, 7552–7555.

(27) (a) Cecchet, F.; Pilling, M.; Hevesi, L.; Schergna, S.; Wong, J. K. Y.; Clarkson, G. J.; Leigh, D. A.; Rudolf, P. *J. Phys. Chem. B.* **2003**, *107*, 10863–10872. (b) Cecchet, F.; Rudolf, P.; Rapino, S.; Margotti, M.; Paolucci, F.; Baggerman, J.; Brouwer, A. M.; Kay, E. R.; Wong, J. K. Y.; Leigh, D. A. *J. Phys. Chem. B* **2004**, *108*, 15192–15199.

(28) (a) Zubavichus, Y.; Zharnikov, M.; Yang, Y.; Fuchs, O.; Umbach, E.; Heske, C.; Ulman, A.; Grunze, M. *Langmuir* **2004**, *20*, 11022–11029. (b) Sarno, D. M.; Jiang, B.; Grosfeld, D.; Afriyie, J. O.; Matienzo, L. J.; Jones, W. E.Jr. *Langmuir* **2000**, *16*, 6191–6199. (c) Graf, N.; Yeğen, E.; Lippitz, A.; Treu, D.; Wirth, T.; Unger, W. E. S. *Surf. Interface Anal.* **2008**, *40*, 180–183.

Table 2. XPS N1s Component Peak Positions (eV) Determined for Nanospheres and Ligand 6

	N1s binding energies (eV)			
samples	$N_{free\ Py}$	$N_{coordinated}$	N_{amide}	$N_{H\text{-}bonded}/N_{protonated}$
Sph-1a (60:40 H_2O/MeOH)		399.6	400.2	401.7
Sph-2a (40:60 H_2O/MeOH)		399.8	400.3	402.0
Sph-1b (60:40 H_2O/MeOH)		399.6	400.2	401.9
(**6**), ligand	398.5		400.1	402.3

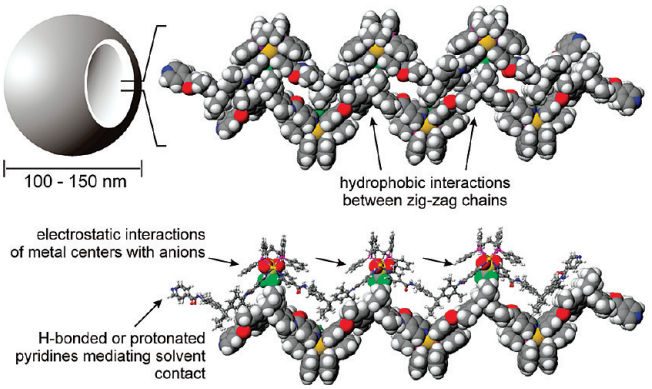

Figure 10. Force-field model of a tetramer of tetrameric chains. Top: Side view showing the good spatial fit between two zigzag chains that are held together by hydrophobic interactions. Bottom: Two chains in a ball-and-stick representation. The anions mediating electrostatic interactions between the chains are highlighted in the space-filling model. They can be located in pockets between metal ions formed through the dppp ligands at the metal centers. The remaining anions may help to connect the chains through hydrogen bonding with the amide protons of adjacent chains. The chains are thus oriented perpendicular to the vesicle surface. The contact between the protic or polar solvent and the interior and exterior surfaces is mediated by hydrogen bonding with terminating pyridine or pyridinium rings.

coordination oligomers destroyed. When instead either triethylamine or sodium hydroxide is added as a base, the suspension of vesicles vanishes in favor of a clear solution. In both cases, the ^{31}P NMR shows only one sharp signal, likely for free metal complexes that may be substituted with hydroxide as the counterions.

11. Structural Model. On the basis of these results, we suggest the structural model shown in Figure 10. Coordination oligomers cross the vesicle wall and can be connected among each other by (i) electrostatic interactions[11] between cationic metal centers and intermittent counterions, (ii) hydrogen bonds between amide groups[29] that may be similar to those found in the crystal structure or between amide N−H atoms and the counterions. (iii) Van der Waals and hydrophobic interactions between the backbones, and (iv) edge-to-face interactions between aromatic rings that have also been observed in the crystal structure of the ligand.[30] On both ends of these oligomers, basic, noncoordinated pyridines exist that are likely partially protonated and form hydrogen bonds with the surrounding water or methanol molecules thus leading to the formation of a wall that is solvated by solvent on both sides.

This structural model is supported by MM3 force field calculations performed with the Cache program package.[31] Figure 10 shows a tetramer of four tetrameric chains, which geometrically fit nicely with each other. In one direction (Figure 10, top), mainly Van der Waals interactions between the nonpolar parts of the banana-shaped dipyridine and the metal-centered dppp ligands mediate vesicle formation. Perpendicular to that direction, pockets are available into which counterions fit so that electrostatic interactions between the cationic metal centers and the counterions connect the individual chains in the assembly. All chains are terminated at both ends with uncoordinated pyridine rings that at least in part can be protonated to yield good interactions with the surrounding water and methanol molecules. In the structure shown in Figure 10 (top), the metals are pointing away from each other. Other structures are also feasible. For example, we obtained a similarly good spatial fit when the upper chain was turned around so that the metal ions of two adjacent chains come closer to each other. Such a simple modeling approach will certainly not provide all structural details and necessarily remains speculative. It remains to be determined where the second counterion could be located in the structure. One possibility is that it is positioned between the chains forming hydrogen bonds to the amides. However, for the time being, such subtle structural details must remain unresolved. The modeling calculations nevertheless provide a reasonable idea of the space requirements of the chains within the vesicle walls.

Conclusions

The formation of vesicles and nanospheres from the metallo-supramolecular oligomers under study here is a quite novel and surprising phenomenon. As our experiments show, a delicate balance of structural details and environmental conditions must be found to make the vesicles emerge. Among the structural details are (i) the banana shape of the ligand which rather leads to the formation of coordination oligomers than to macrocycles, (ii) a suitable distribution of nonpolar parts within the ligand and the metal connector (e.g., dppp vs en ligand), and (iii) even the position of the nitrogen atom in the pyridine rings. The environmental conditions that need to be controlled are the solvent mixture, the pH, and if depositing the vesicles on a surface, its exact nature.

The assembly process leading to the vesicles and nanospheres is a hierarchical one: First, coordination oligomers self-assemble from the building blocks, followed by a second assembly step in which they are integrated to yield the vesicles. This interpretation is supported by the finding that it did not matter how the vesicle suspension was prepared. Preforming the oligomers in dichloromethane followed by precipitation, isolation, and

(29) Bisson, A. P.; Carver, F. J.; Eggleston, D. S.; Haltiwanger, R. C.; Hunter, C. A.; Livingstone, D. L.; McCabe, J. F.; Rotger, C.; Rowan, A. E. *J. Am. Chem. Soc.* **2000**, *122*, 8856–8868.
(30) (a) Blokzijl, W.; Engberts, J. B. F. N. *Angew. Chem.* **1993**, *115*, 796–800.
(31) *CACHE 5.0 for Windows*; Fujitsu Ltd.: Krakow, Poland, **2001**.

dissolution in methanol/water mixtures lead to the same result as mixing the individual building blocks directly in this solvent mixture.

Experimental Section

1. General Methods. All self-assembly reactions were conducted under a dry argon atmosphere using Schlenk techniques. NMR spectra were acquired on Bruker DRX 500 (^{1}H (500 MHz), ^{13}C (125 MHz), ^{19}F (470 MHz), and ^{31}P (202 MHz) nuclei) and DPX 400 ^{1}H (400 MHz) and ^{13}C (100 MHz) spectrometers at room temperature. All ^{1}H chemical shifts are reported in parts per million relative to residual nondeuterated solvent signals as the internal standard: $CDCl_3$ (7.24 ppm), [D_6]DMSO (2.50 ppm), [D_7]DMF (2.75 ppm). ^{13}C chemical shifts are given in parts per million relative to the carbon resonance of the deuterated NMR solvent: $CDCl_3$ (77.0 ppm), [D_6]DMSO (39.52 ppm), [D_7]DMF (29.76 ppm). ^{31}P chemical shifts are provided in parts per million relative to an external 86% H_3PO_4 (0 ppm) standard. ^{19}F chemical shifts are reported relative to external $CFCl_3$ (0.00 ppm). Routine mass spectra were recorded on an Agilent 6210 ESI-TOF mass spectrometer (Agilent Technologies). Mass spectra of the assemblies were recorded with a Varian/IonSpec QFT-7 FTICR mass spectrometer (Varian Inc.) equipped with a superconducting 7 T magnet and a Micromass Z-spray ESI ion source (Waters Inc.) utilizing a stainless steel capillary with a 0.75 mm inner diameter. 150 μM analyte solutions in acetone were introduced into the ion source with a syringe pump (Harvard Apparatus) at flow rates of approximately 2 μL min^{-1}. Typical ionization parameters were: capillary voltage: 3.2 kV; sample cone: −32 V; extractor cone: −8 V; source temperature: 45 °C; temperature of desolvation gas: 40 °C. No nebulizer gas was used for the experiments. The ions were introduced into the FTICR analyzer cell, which was operated at pressures below 1×10^{-9} mbar, and detected by a standard excitation and detection sequence. Melting points were obtained with a Büchi-SMP-20 and were not corrected. All reagents used were analytical grade; solvents were purchased from Aldrich, LG Promochem, and Roth.

2. Syntheses of Ligands. Acid chlorides were prepared by standard reaction with thionyl chloride and were used without further purification. 4,4′-(Cyclohexane-1,1′-diyl)-bis-(2,6-dimethylaniline) **1** (Hunter's diamine) was synthesized according to the literature.[14]

*N-(4-(1-(4-Amino-3,5-dimethylphenyl)cyclohexyl)-2,6-dimethylphenyl) Isonicotinamide **4***. Hunter's diamine **1** (4.06 g, 12.6 mmol) is placed in a 100 mL, three-necked round-bottomed reaction flask and filled with dry CH_2Cl_2 (50 mL) under argon. Triethylamine (TEA; 7.0 mL, 4 equiv) was added to the solution followed by isonicotinoyl chloride **2** (1.87 g, 1 equiv). The reaction was allowed to stir at r.t. overnight. The content was transferred into an extraction funnel and washed with 3 × 200 mL of water. The organic phase was then dried over $MgSO_4$, the $MgSO_4$ filtered off and the solvent removed in vacuo. Column chromatography on silica with CH_2Cl_2:MeOH (5:1) as the eluent afforded pure product.

White solid, 70%. R_f = 0.45. CH_2Cl_2:MeOH = 5:1 (SiO_2). Mp = 215 °C. ^{1}H NMR (400 MHz, [D_6]DMSO, 25 °C, TMS): δ (ppm) = 9.91 (s, 1H, H_{amide}), 8.77 (d, 2H, $H_{pyridine(\alpha)}$), 7.86 (d, 2H, $H_{pyridine(\beta)}$), 7.01 (s, 2H, H_{phenyl}), 6.76 (s, 2H, H_{phenyl}), 4.32 (b, 2H, H_{amine}), 2.17 (b, 4H, $H_{aliphatic}$), 2.12 (s, 6H, CH_3), 2.04 (s, 12H, CH_3), 1.46 (b, 6H, $H_{aliphatic}$). ^{13}C NMR (100 MHz, CD_3OD, 25 °C): δ (ppm) = 164.00, 150.89, 150.86, 148.77, 142.01, 141.95, 135.58, 135.12, 132.01, 126.66, 126.58, 121.93, 120.81, 44.58, 36.98, 23.17, 21.27, 18.91, 18.76, 14.60. MS (ESI-TOF): m/z = 428.27 $[M+H]^+$, 450.25 $[M+Na]^+$, 466.23 $[M+K]^+$.

*N,N′-(4,4′-(cyclohexane-1,1-diyl)-bis-(2,6-dimethyl-4,1-phenylene)) diisonicotinamide **6***. The same procedure as that used for the synthesis of **4** was used. However, a larger amount of isonicotinoyl chloride **2** (6.69 g, 3 equiv) was added in six portions over 1 h. The raw product was purified by column chromatography on silica with CH_2Cl_2:MeOH (9:1) as the eluent. For the preparation of assemblies, it is recommended to further purify the ligand by chromatography on basic Al_2O_3 (same mobile phase) in order to remove any HCl left in the product as hydrochloride.

White solid, 75%. R_f = 0.54. CH_2Cl_2:MeOH = 9:1 (SiO_2). Mp = 185 °C. ^{1}H NMR (400 MHz, [D_6]DMSO, 25 °C, TMS): δ (ppm) = 9.71 (s, 2H, H_{amide}), 8.69 (d, 4H, $H_{pyridine(\alpha)}$), 7.84 (d, 4H, $H_{pyridine(\beta)}$), 7.01 (s, 4H, H_{phenyl}). 2.17 (b, 4H, $H_{aliphatic}$), 2.12 (s, 12H, H_{methyl}), 1.46 (b, 6H, $H_{aliphatic}$). ^{13}C NMR (100 MHz, CD_3OD, 25 °C): δ (ppm) = 166.5, 151.8, 149.7, 148.6, 144.8, 136.6, 132.2, 128.4, 127.0, 46.8, 38.2, 27.6, 24.2, 18.9. MS (ESI-FTICR): m/z = 533.3 $[M+H]^+$, 555.28 $[M+Na]^+$, 1065.6 $[M_2+H]^+$ dimer, 1598.96 $[M_3+2H]^+$ trimer.

*N-(4-(1-(4-Benzamido-3,5-dimethylphenyl)cyclohexyl)-2,6-dimethylphenyl) Isonicotinamide **5***. Compound **4** (0.36 g, 0.84 mmol) was reacted in the presence of 0.70 mL TEA in CH_2Cl_2 as described above with benzoyl chloride (0.39 g, 4 equiv). Purification was accomplished by column chromatography on silica with CH_2Cl_2:MeOH (9:1) as the eluent. To obtain a chloride-free ligand, chromatography on basic Al_2O_3 using the same solvent system is recommended.

White solid, 72%. R_f = 0.60. CH_2Cl_2:MeOH = 9:1 (SiO_2). Mp = 175 °C. ^{1}H NMR (400 MHz, [D_6]DMSO, 25 °C, TMS): δ (ppm) = 9.92 (s, 1H, H_{amide}), 9.61 (s, 1H, H_{amide}), 8.77 (d, 2H, $H_{pyridine(\alpha)}$), 7.95 (t, 2H, $H_{benzene}$), 7.86 (d, 2H, $H_{pyridine(\beta)}$), 7.51 (m, 4H, $H_{benzene}$), 7.11 (s, 2H, H_{phenyl}), 7.09 (s, 2H, H_{phenyl}), 2.28 (b, 6H, $H_{aliphatic}$, CH_2), 2.15 (b, 12H, CH_3), 1.52 (b, 6H, $H_{aliphatic}$, CH_2). ^{13}C NMR (100 MHz, CD_3OD, 25 °C): δ (ppm) = 165.5, 163.9, 150.9, 141.9, 135.63, 135.47, 134.94, 133.11, 132.39, 129.78, 129.09, 128.96, 127.93, 126.70, 126.57, 121.91, 45.53, 21.57, 21.28, 19.00, 18.93. MS (ESI-TOF): m/z = 532.3 $[M+H]^+$, 554.3 $[M+Na]^+$, 570.3 $[M+K]^+$.

*Ethylated Control Compounds **7** and **9***. Ligand **6** (2.49 g, 7.73 mmol) is placed in a 100 mL, three-necked round-bottomed flask filled with dry DMF (100 mL) under argon. The reaction flask is placed on an ice bath. Afterward, 10 mL DMF solution of ethyltriflate (EtOTf; 1.0 mL, 7.73 mmol) was added to the mixture. The reaction was allowed to stir at r.t. for 2 days. DMF was removed in vacuo and the residue was purified by column chromatography on basic Al_2O_3 with CH_2Cl_2:MeOH (9:1) as the eluent. Monotriflate salt **7** was obtained as a first fraction, bis-triflate salt **9** as a second fraction from the column.

*Mono(4,4′-(4,4′-(cyclohexane-1,1-diyl)bis(2,6-dimethyl-4,1 phenylene)) Bis(azanediyl) bis(oxomethylene)-mono(1-ethylpyridinium)) Mono(trifluoromethanesulfonate) **7***. White solid, 72%. R_f = 0.6. CH_2Cl_2:MeOH = 9:1 (Al_2O_3). Mp = 182 °C. ^{1}H NMR (400 MHz, [D_6]DMSO, 25 °C, TMS): δ (ppm) = 10.39 (s, 1H, H_{amide}), 9.92 (s, 1H, H_{amide}), 9.30 (d, 2H, $H_{pyridine(\alpha)}$), 8.78 (d, 2H, $H_{pyridine(\alpha)}$), 8.53 (d, 2H, $H_{pyridine(\beta)}$), 7.85 (d, 2H, $H_{pyridine(\beta)}$), 7.14 (s, 2H, H_{phenyl}), 7.10 (s, 2H, H_{phenyl}), 4.73 (t, 3H, H_{ethyl}), 2.28 (b, 6H, $H_{aliphatic}$, CH_2), 2.15 (s, 6H, CH_3), 2.12 (s, 6H, CH_3), 1.52 (b, 6H, $H_{aliphatic}$, CH_2). ^{13}C NMR (100 MHz, [D_6]DMSO, 25 °C): δ (ppm) = 165.5, 163.9, 150.9,

146.25, 146.23, 141.88, 135.51, 135.31, 132.46, 131.59, 127.50, 126.92, 121.90, 119.60, 110.55, 45.37, 36.62, 29.35, 23.16, 18.92, 16.82. MS (ESI-TOF): m/z = 561.32 $[M\text{-}OTf]^+$.

*Mono(4,4′-(4,4′-(cyclohexane-1,1-diyl)bis(2,6-dimethyl-4,1 phenylene)) Bis(azanediyl) bis(oxomethylene)-bis(1-ethylpyridinium)) Bis(trifluoromethanesulfonate) **9***. White solid, 20%. R_f = 0.6. CH_2Cl_2:MeOH = 9:1 (Al_2O_3). Mp = 172 °C. ^{1}H NMR (400 MHz, [D_6]DMSO, 25 °C, TMS): δ (ppm) = 10.40 (s, 2H, H_{amide}), 9.31 (d, 4H, $H_{pyridine(\alpha)}$), 8.78 (d, 4H, $H_{pyridine(\beta)}$), 7.13 (s, 4H, H_{phenyl}), 4.73 (t, 6H, H_{ethyl}), 2.28 (b, 6H, $H_{aliphatic}$, CH_2), 2.15 (s, 6H, CH_3), 2.12 (s, 6H, CH_3), 1.52 (b, 6H, $H_{aliphatic}$, CH_2). ^{13}C NMR (100 MHz, [D_6]DMSO, 25 °C): δ (ppm) = 163.9, 150.9, 148.55, 146.20, 135.51, 131.59, 127.50, 126.92, 119.59, 118.75, 45.40, 23.14, 20.40, 18.86, 16.82.

*N-(2,6-Dimethyl-4-(1-(3,5-dimethyl-4-(nicotinamido)phenyl)cyclohexyl)phenyl)nicotinamide **8***. The same procedure as described above for the synthesis of **6** was applied using nicotinoyl chloride instead of isonicotinoyl chloride. The raw product was purified by column chromatography on silica with CH_2Cl_2:MeOH (22:1) as the eluent. The second fraction corresponds to the desired product. Chromatography on basic Al_2O_3 removes hydrochlorides that may interfere with the assembly formation.

White solid, 75%. R_f = 0.45. CH_2Cl_2:MeOH = 22:1 (SiO_2). Mp = 185 °C. ^{1}H NMR (400 MHz, [D_6]DMSO, 25 °C, TMS): δ (ppm) = 9.83 (s, 2H, H_{amide}), 9.13 (s, 2H, $H_{pyridine}$), 8.75 (d, 2H, $H_{pyridine}$), 8.28 (d, 2H, $H_{pyridine}$), 7.58 (t, 2H, $H_{pyridine}$), 7.10 (s, 4H, H_{phenyl}), 2.23 (s, 4H, $H_{aliphatic}$), 2.16 (s, 12H, H_{methyl}), 1.48 (b, 6H, $H_{aliphatic}$). ^{13}C NMR (100 MHz, [D_6] DMSO, 25 °C): δ (ppm) = 164.0, 152.6, 149.0, 147.3, 135.7, 135.5, 132.6, 130.5, 126.7, 124.2, 45.3, 36.6, 23.1, 21.2, 18.9. MS (ESI-TOF): m/z = 533.29 $[M+H]^+$, 555.27 $[M+Na]^+$, 571.24 $[M+K]^+$.

3. Preparation of Assemblies 11a,b−14a,b and 16a,b. Oligomers **11a** and **11b** were prepared by mixing equimolar amounts of the corresponding (dppp)M$(OTf)_2$ complexes (**10a**: M = Pd^{II}, **10b**: M = Pt^{II}) and of ligand **6** were mixed in dichloromethane and the mixture is stirred for 2 h. Finally, slow addition of diethyl ether to the reaction mixture resulted in a white precipitate of **11a** and **11b**, with yield of 95% and 90%, respectively. NMR analysis of the isolated oligomers and of the mixture before isolation did not show significant differences so that we can assume the oligomers to form almost quantitatively. The other complexes **12a,b**, **13a,b**, and **14a,b** were synthesized following the same procedure, however, without isolation; for the preparation of **16a,b**, water was used as the solvent for oligomer generation.

11a: White solid, 95%. ^{1}H NMR (400 MHz, [D_7]DMF, 25 °C, TMS): δ (ppm) = 9.92 (s, 2H, H_{amide}), 9.14 (b, 4H, $H_{pyridine}$), 7.87−7.82 (m, 16H, $H_{dppp\text{-}meta}$ + $H_{pyridine}$), 7.63 (b, 5H, $H_{dppp\text{-}para}$), 7.52 (m, 10H, $H_{dppp\text{-}ortho}$), 7.20 (s, 4H, H_{phenyl}), 3.30 (b, 6H, H_{dppp}), 2.32 (b, 8H, CH_2 $H_{cyclohexyl}$), 2.18 (s, 12H, CH_3), 1.53 (b, 8H, CH_2 $H_{cyclohexyl}$). ^{13}C NMR (100 MHz, [D_6] DMSO, 25 °C): δ (ppm) = 155.07, 151.39, 147.52, 139.18, 137.36, 136.01, 136.62,133.57, 130.53, 130.00, 129.55, 127.71, 126.80, 124.24, 49.04, 40.39, 30.12, 26,87, 25.78, 25.44, 21.97. ^{31}P NMR (202 MHz, [D_7]DMF, 25 °C): δ (ppm) = 11.16, 5.67. ^{19}F NMR (470 MHz, [D_7]DMF, 25 °C): δ (ppm) = −79.06. MS (ESI-FTICR, acetone): m/z = 1199.4 $[ML(OTf)]^+$, and $[M_2L_2(OTf)]^{2+}$.

11b: White solid, 90%. ^{1}H NMR (400 MHz, [D_7]DMF, 25 °C TMS): δ (ppm) = 9.96−9.91 (m, 2H, H_{amide}), 9.26 (b, 4H, $H_{pyridine}$), 8.83 (d, $H_{pyridine\text{-}free}$), 7.85 (m, 14H, $H_{dppp\text{-}meta}$ + $H_{pyridine}$), 7.55 (m, 5H, $H_{dppp\text{-}para}$), 7.48 (m, 10H, $H_{dppp\text{-}ortho}$), 7.22−7.19 (m, 4H, H_{phenyl}), 2.32 (b, 6H, CH_2 $H_{cyclohexyl}$), 2.15 (s, 6H, CH_3), 2.13 (s, 6H, CH_3), 1.53 (b, 8H, CH_2 $H_{cyclohexyl}$). ^{13}C NMR (100 MHz, [D_6]DMSO, 25 °C): δ (ppm) = 168.40, 166.73, 166.25, 165.74, 165.66, 156.08, 155.64, 155.33, 151.95, 148.38, 148.23, 148.05, 146.28, 139.94, 139.64, 138.10, 136.68, 136.28, 136.11, 131.21, 129.42, 126.29, 40.99, 30.62, 27.48, 25.79, 23.29, 23.24, 23.07, 22.08, 13.54. MS (ESI-FTICR, acetone): m/z = 1288.5 Da $[ML(OTf)]^+$, and $[M_2L_2(OTf)]^{2+}$. ^{31}P NMR (202 MHz, [D_7]DMF, 25 °C): δ (ppm) = −14.05 (open assemblies (L_2M): $^1J_{Pt-P}$ = 3041 Hz), −11.82 (mono metal coordination, (LM); −10.7 (free (dppp)Pt$(OTf)_2$, $^1J_{Pt-P}$ = 3646 Hz), −9.47 (cyclic assemblies, L_2M_2). ^{19}F NMR (470 MHz, [D_7] DMF, 25 °C): δ (ppm) = −79.09. MS (ESI-FTICR, acetone): m/z = 1288.4 $[ML\text{-}OTf]^+$ and $[M_2L_2\text{-}OTf]^{2+}$.

12a: ^{1}H NMR (400 MHz, [D_7]DMF, 25 °C, TMS): δ (ppm) = 9.75 (s, 2H, H_{amide}), 9.25 (s, 2H, H_{amide}), 8.47 (d, 4H, $H_{pyridine}$), 7.87 (b, 4H, H_{dppp}), 7.71−7.40 (b, 20H, $H_{pyridine}$ + $H_{dppp\text{-}pmeta}$ + $H_{dppp\text{-}para}$ + $H_{dppp\text{-}ortho}$), 7.24 (s, 8H, H_{phenyl}), 3.31 (b, 4H, CH_2 H_{dppp}), 2.37 (b, 6H, CH_2 $H_{cyclohexyl}$), 2.22 (s, 24H, CH_3), 1.58 (b, 6H, CH_2 $H_{cyclohexyl}$), 1.51 (b, 3H, CH_2 $H_{cyclohexyl}$). ^{13}C NMR (100 MHz, CD_3OD, 25 °C): δ (ppm) = 152.29, 150.01, 147.23, 136.52, 135.29, 135.27, 133.34, 132.58, 132.17, 129.68, 129.57, 126.61, 126.54, 125.28, 124.32, 122.42, 118.91, 59.95, 45.06, 36.51, 26.16, 22.90, 21.81, 21.55, 20.20, 18.16, 17.61, 13.85. ^{31}P NMR (202 MHz, [D_7]DMF, 25 °C): δ (ppm) = 14.25, 11.13. ^{19}F NMR (470 MHz, [D_7]DMF, 25 °C): δ (ppm) = −78.95. MS (ESI-FTICR, acetone): m/z = 532.3 $[LH]^+$, 1063.6 $[L_2H]^+$, 1198.3 $[ML(OTf)]^+$, 1728.6 $[ML_2(OTf)]^+$.

12b: ^{1}H NMR (400 MHz, [D_7]DMF, 25 °C, TMS): δ (ppm) = 9.71 (s, 2H, H_{amide}), 9.57 (d, 2H, $H_{pyridine}$), 9.27 (s, 2H, H_{amide}), 8.53 (d, 2H, $H_{pyridine}$), 7.76 (b, 2H, H_{dppp}), 7.71−7.30 (b, 20H, $H_{pyridine}$ + $H_{dppp\text{-}pmeta}$ + $H_{dppp\text{-}para}$ + $H_{dppp\text{-}ortho}$), 7.24 (b, 8H, H_{phenyl}), 3.24 (b, 2H, CH_2 H_{dppp}), 2.38 (b, 2H, CH_2 $H_{cyclohexyl}$), 2.19 (s, 12H, CH_3), 1.40 − 1.65 (b, 8H, CH_2 $H_{cyclohexyl}$). ^{13}C NMR (100 MHz, CD_3OD, 25 °C): δ (ppm) = 160.71, 152.31, 150.70, 147.51, 138.19, 135.21, 135.19, 134.20, 133.60, 133.22, 131.94, 129.34, 127.10, 126.50, 124.31, 122.33, 120.53, 118.67, 112.11, 59.96, 45.41, 36.51, 26.01, 22.89, 21.48, 20.21, 18.15, 17.51, 14.11. ^{31}P NMR (202 MHz, [D_7] DMF, 25 °C): δ (ppm) = −13.83 (L_2M, $^1J_{Pt-P}$ = 3053 Hz), −10.15 (LM). ^{19}F NMR (470 MHz, [D_7]DMF, 25 °C): δ (ppm) = −78.95. MS (ESI-FTICR, acetone): m/z = 1287.3 $[ML(OTf)]^+$, 1818.5 $[ML_2(OTf)]^+$.

13a: ^{1}H NMR (400 MHz, [D_7]DMF, 25 °C, TMS): δ (ppm) = 9.92 (s, 2H, H_{amide}), 9.60 (s, 2H, H_{amide}), 9.10 (b, 4H, $H_{pyridine}$), 8.09 (d, 4H, $H_{pyridine}$), 7.85 (b, 20H, $H_{dppp\text{-}pmeta}$), 7.65 (b, 10H, $H_{dppp\text{-}para}$), 7.55 (m, 20H, $H_{dppp\text{-}ortho}$), 7.22 (s, 4H, H_{phenyl}), 7.19 (s, 4H, H_{phenyl}), 3.25 (b, 6H, CH_2 H_{dppp}), 2.34 (b, 10H, CH_2), 2.25 (s, 12H, CH_3), 2.19 (s, 12H, CH_3), 1.55 (b, 12H, CH_2 $H_{cyclohexyl}$). ^{13}C NMR (100 MHz, CD_3OD, 25 °C): δ (ppm) = 165.54, 151.23, 147.59, 146.84, 143.88, 135.46, 135.19, 133.59, 133.19, 132.73, 131.96, 131.49, 129.68, 128.55, 127.69, 126.62, 126.39, 125.85, 124.02, 123.17, 119.97, 45.07, 36.47, 26.33, 26.20, 22.95, 18.23, 18.03. ^{31}P NMR (202 MHz, [D_7]DMF, 25 °C): δ (ppm) = 15.55. ^{19}F NMR (470 MHz, [D_7]DMF, 25 °C): δ (ppm) = −78.51. MS (ESI-FTICR, acetone): m/z = 532.3 $[LH]^+$, 1063.6 $[L_2H]^+$, 1198.3 $[ML(OTf)]^+$, 1728.6 $[ML_2(OTf)]^+$.

13b: ^{1}H NMR (400 MHz, [D_7]DMF, 25 °C, TMS): δ (ppm) = 9.98 (s, 1H, H_{amide}), 9.94 (s, 1H, H_{amide}), 9.60 (d, 2H, $H_{pyridine}$), 9.27 (d, 2H, $H_{pyridine}$), 9.05 (d, 2H, $H_{pyridine}$), 8.08 (d, 4H, $H_{pyridine}$), 8.03−7.41 (b, 50H, $H_{pyridine}$ + $H_{dppp\text{-}pmeta}$ + $H_{dppp\text{-}para}$ + $H_{dppp\text{-}ortho}$), 7.32−7.19 (m, 8H, H_{phenyl}), 3.24 (b, 6H, CH_2 H_{dppp}), 2.34 (b, 10H, CH_2 $H_{cyclohexyl}$), 2.23 (s, 12H, CH_3), 2.17 (s, 12H, CH_3), 1.55 (b, 12H, CH_2 $H_{cyclohexyl}$). ^{13}C NMR (100 MHz, CD_3OD, 25 °C): δ (ppm) =

165.54, 151.30, 146.83, 144.57, 135.45, 135.18, 133.61, 133.19, 131.78, 131.51, 129.56, 128.56, 127.68, 126.64, 126.39, 123.18, 121.10, 119.98, 45.06, 36.47, 26.21, 26.19, 22.94, 18.22, 18.04, 18.03. ^{31}P NMR (202 MHz, [D_7] DMF, 25 °C): δ (ppm) = −13.34 (L_2M: $^1J_{Pt-P}$ = 3053 Hz), −11.08 (LM), −9.93 (free (dppp)Pt $(OTf)_2$: $^1J_{Pt-P}$ = 3646 Hz). ^{19}F NMR (470 MHz, [D7]DMF, 25 °C): δ (ppm) = −78.68. MS (ESI-FTICR, acetone): m/z = 1287.3 [ML $(OTf)]^+$, 1818.5 $[ML_2(OTf)]^+$.

14a: ^{1}H NMR (400 MHz, [D_6]DMSO, 25 °C, TMS): δ (ppm) = 10.37 (s, 1H, H_{amide}), 9.88 (s, 1H, H_{amide}), 9.30 (d, 2H, $H_{pyridine}$), 8.89 (b, 2H, $H_{pyridine}$), 8.52 (d, 2H, $H_{pyridine}$), 7.73 (b, 8H, $H_{dppp\text{-}pmeta}$), 7.58 (b, 4H, $H_{dppp\text{-}para}$), 7.48 (m, 8H, $H_{dppp\text{-}ortho}$), 7.11 (s, 2H, H_{phenyl}), 7.10 (s, 2H, H_{phenyl}), 4.71 (m, 3H, CH_3), 3.00 (b, 4H, CH_2 H_{dppp}), 2.34 (b, 10H, CH_2), 2.26 (s, 12H, CH_3), 2.20 (s, 12H, CH_3), 1.59 (t, 2H, CH_2), 1.55 (b, 6H, CH_2 $H_{cyclohexyl}$). ^{31}P NMR (202 MHz, [D_6]DMSO, 25 °C): δ (ppm) = 15.95 and 9.01. ^{19}F NMR (470 MHz, [D_6]DMSO, 25 °C): δ (ppm) = −77.63.

14b: ^{1}H NMR (400 MHz, [D_6]DMSO, 25 °C, TMS): δ (ppm) = 10.34 (s, 1H, H_{amide}), 9.94 (s, 1H, H_{amide}), 9.82 (s, 1H, H_{amide}), 9.30 (d, 2H, $H_{pyridine}$), 9.03 (d, 2H, $H_{pyridine}$), 8.88 (d, 2H, $H_{pyridine}$), 8.52 (d, 2H, $H_{pyridine}$), 7.87−7.31 (m, 50H, $H_{pyridine}$ + $H_{dppp\text{-}pmeta}$ + $H_{dppp\text{-}para}$ + $H_{dppp\text{-}ortho}$), 7.12 (s, 8H, H_{phenyl}), 7.09 (d, 8H, H_{phenyl}), 4.71 (m, 3H, CH_3), 3.24 (b, 6H, CH_2 H_{dppp}), 2.98 (b, 10H, CH_2 $H_{cyclohexyl}$), 2.26 (b, 12H, CH_3), 2.17 (s, 12H, CH_3), 2.13 (s, 12H, CH_3), 2.06 (s, 12H, CH_3), 1.59 (t, 2H, CH_2), 1.48 (b, 12H, CH_2 $H_{cyclohexyl}$). ^{31}P NMR (202 MHz, [D_6] DMSO, 25 °C): δ (ppm) = −13.13 (L_2M: $^1J_{Pt-P}$ = 3053 Hz), −9.82 (d) and −10.75 (d) (LM), −9.93 (free (dppp)Pt $(OTf)_2$: $^1J_{Pt-P}$ = 3646 Hz). ^{19}F NMR (470 MHz, [[D_6] DMSO, 25 °C): δ (ppm) = −77.62.

16a: A volume of 1 mL of a 0.01 M solution of **6** and **15a** (5.33 mg, 0.01 mol) was heated in a vial to 80 °C for 30 min. ^{1}H NMR (400 MHz, [D_6] DMSO, 25 °C, TMS): δ (ppm) = 10.22 (s, 1H, H_{amide}), 10.15 (s, 1H, H_{amide}), 10.08 (s, 2H, H_{amide}), 9.98 (s, 1H, H_{amide}), 9.06 (d, 2H, $H_{pyridine}$), 9.01 (d, 1H, $H_{pyridine}$), 8.93 (d, 1H, $H_{pyridine}$), 8.78 (d, 4H, $H_{pyridine}$), 8.16 (m, 2H, $H_{pyridine}$), 8.07 (m, 1H, $H_{pyridine}$), 7.95 (m, 1H, $H_{pyridine}$), 7.86 (m, 4H, $H_{pyridine}$), 7.13 (s, 1H, H_{phenyl}), 7.11 (s, 1H, H_{phenyl}), 7.10 (s, 1H, H_{phenyl}), 7.08 (s, 1H, H_{phenyl}), 6.38 (b, 4H, NH_2), 6.35 (b, 1H, NH_2), 6.09 (b, 1H, NH_2), 6.02 (b, 1H, NH_2), 2.68 (b, 4H, CH_2), 2.64 (b, 1H, CH_2), 2.54 (b, 1H, CH_2), 2.42 (b, 1H, CH_2), 2.16 (s, 4H, CH_3), 2.15 (s, 9H, CH_3), 2.14 (s, 9H, CH_3), 2.12 (s, 9H, CH_3), 1.50 (b, 12H, CH_2 $H_{cyclohexyl}$). MS (ESI-FTICR, acetone): m/z = 532.3 $[LH]^+$, 698.3 $[ML]^+$, $[M_2L_2]^+$, 615.3 $[ML_2]^{2+}$.

16b: A volume of 1 mL of a 0.01 M solution of **6** and **15b** (5.33 mg, 0.01 mol) was heated in a vial to 80 °C for 30 min. ^{1}H NMR (400 MHz, [D_6] DMSO, 25 °C, TMS): δ (ppm) = 10.14 (s, 2H, H_{amide}), 10.07 (s, 2H, H_{amide}), 9.89 (s, 1H, H_{amide}), 9.81 (s, 1H, H_{amide}), 9.02 (d, 2H, $H_{pyridine}$), 8.92 (d, 3H, $H_{pyridine}$), 8.77 (d, 1H, $H_{pyridine}$), 8.50 (d, 1H, $H_{pyridine}$), 8.06 (m, 2H, $H_{pyridine}$), 7.96 (m, 3H, $H_{pyridine}$), 7.85 (m, 1H, $H_{pyridine}$), 7.33 (m, 1H, $H_{pyridine}$), 7.11 (s, 1H, H_{phenyl}), 7.09 (s, 2H, H_{phenyl}), 7.07 (s, 1H, H_{phenyl}), 7.06 (s, 4H, H_{phenyl}), 7.02 (s, 1H, H_{phenyl}), 6.40 (b, 3H, CH_2), 6.38 (b, 2H, CH_2), 6.18 (b, 1H, CH_2), 5.40 (b, 1H, CH_2), 2.66 (b, 6H, CH_2), 2.42 (b, 2H, CH_2), 2.26 (b, 8H, CH_2), 2.15 (s, 1H, CH_3), 2.14 (s, 4H, CH_3), 2.12 (s, 3H, CH_3), 2.10 (s, 12H, CH_3), 1.50 (b, 8H, CH_2 $H_{cyclohexyl}$), 1.47 (b, 4H, CH_2 $H_{cyclohexyl}$). MS (ESI-FTICR, acetone): m/z = 532.3 $[LH]^+$, 787.3 $[ML]^+$, $[M_2L_2]^+$, 659.8 $[ML_2]^{2+}$.

Acknowledgment. The authors thank Dr. A. Schäfer for NMR spectroscopic experiments, Meike Roskamp for help with powder X-ray experiments, and Prof. Dr. Jürgen Fuhrhop for helpful discussions. Funding by the Deutsche Forschungsgemeinschaft (DFG) and the Fonds der Chemischen Industrie (FCI) is acknowledged.

Supporting Information Available: Additional TEM experiments, crystal data of the ligand **6**, syntheses of the bidentate and monodentate ligands, self-assemblies and nanospheres, X-ray diffractograms of the assemblies and nanospheres, XPS spectra of the free metal complex precursors (PDF). This material is available free of charge via the Internet at http://pubs.acs.org.